Photochemical & Photobiological Sciences
https://doi.org/10.1007/s43630-026-00910-3

BRIEF REPORT

Formation and cellular uptake of Bleomycin saccharide decorated molecular spherical nucleic acids evaluated by time-resolved fluorescence spectroscopy

Toni Laine[1] · Iida Kähärä[2] · Ann-Mari Yliperttula[1] · Ezgi Özliseli[3] · Saara Siekkinen[1] · Emilia Löfman[2] · Ekaterina Lisitsyna[2] · Annika Gerlander[2] · Vijay Gulumkar[1] · Elina Vuorimaa-Laukkanen[2] · Jessica M. Rosenholm[3] · Marjo Yliperttula[4] · Päivi Poijärvi-Virta[1] · Pasi Virta[1]

Received: 27 January 2026 / Accepted: 20 April 2026

Abstract
Oligonucleotide-carbohydrate conjugates is an efficient strategy to provide cell-specific delivery of oligonucleotides. Combining the multivalent nature of molecular spherical nucleic acids (MSNAs) with a proper glyco-decoration results in multiglyco-oligonucleotide constructs, which could potentially increase the sugar-based cell surface recognition and widen the scope of sugars applied for delivery. On the other hand, MSNAs are prone to scavenger A-receptor-mediated endocytosis, the strength of which can hardly be compensated by the sugar-mediated delivery. In this report, the formation of bleomycin saccharide-decorated MSNAs was evaluated by steady-state and time-resolved spectroscopies, revealing significant effects on the fluorescence quantum yields and negative cooperativity. Cellular uptake of the MSNAs in cancerous 22Rv1 and PC3 cell-lines was evaluated by fluorescence-lifetime imaging microscopy (FLIM), wide-field microscopy, and flow cytometry. In addition, optimized synthesis and further characterization (homogeneity and molecular mass evaluation, DNase I stability) of these hybridization-mediated macromolecular glycoclusters, consisting of 36 mono/disaccharide units, were described.

Keywords Molecular spherical nucleic acids · Antisense oligonucleotide · Bleomycin · Carbohydrate conjugates · Fluorescence lifetime microscopy · Time-resolved fluorescence

1 Introduction

Conjugation of oligonucleotides to carbohydrates is a potential method to increase their tissue-specific delivery and cellular uptake via receptor-mediated endocytosis. For example, conjugation to *N*-acetylgalactosamine (GalNAc) [1], which results in targeted delivery to hepatocytes via asialoglycoprotein receptors, is applied in FDA (U.S. Food and Drug Administration) approved small interfering RNAs (siRNAs): Givosiran, Lumasiran, Inclisinar, and Vutrisinar [2]. Since many carbohydrate–protein interactions are multivalent, multiple copies of the carbohydrate, resulting in glycoclusters, are usually needed for sufficient cell-specific targeting [2, 3]. The biodistribution properties may also change due to the altered binding of the conjugates to plasma proteins.

Bleomycin (BLM) is a glycopeptoid-derivative that is used in cancer treatment. Its targeting to tumors is

Toni Laine and Iida Kähärä contributed equally to this work

✉ Pasi Virta
pamavi@utu.fi

[1] Department of Chemistry , University of Turku , FI-20500 Turku, Finland

[2] Faculty of Engineering and Natural Sciences Chemistry and Advanced Materials , Tampere University , Tampere, FinlandFI-33720

[3] Department of Natural and Health Sciences Faculty of Science and Engineering Pharmaceutical Sciences Laboratory , Åbo Akademi University , Turku FI-20500, Finland

[4] Division of Pharmaceutical Biosciences Faculty of Pharmacy, University of Helsinki, Helsinki FI-00014, Finland

Published online: 12 May 2026

achieved through a bleomycin disaccharide (i.e. 2-*O*-(3-*O*-carbamoyl-α-D-mannopyranosyl)-L-gulopyranose) while the peptoid part is responsible for the cytotoxicity [4–6]. BLM saccharides have been shown to increase uptake in several cancer cell lines, including breast cancer and prostate cancer [7–10]. The cellular uptake in tumor cells is markedly better than in equivalent non-cancerous cell lines, proving that the uptake is selective to tumor cells [7, 8]. The reason behind the selectivity is expected to be related to glucose transporters, which are upregulated in tumors [8, 9]. The cellular uptake of BLM is dependent on the placement and stereochemistry of the disaccharide as well as the placement of the carbamoyl group [9, 11]. The monosaccharide carbamoylmannose by itself is also capable of enhancing uptake in tumor cells [10]. Additionally, it has been shown that glycoclusters consisting of three BLM saccharides can enhance cellular uptake in tumor cells [8, 10, 11], providing evidence that the interactions of BLM saccharides with cell surface receptors are multivalent. BLM saccharides have shown potential as targeting moieties for molecules other than BLM, including dyes [7, 10, 11], microbubbles [12] and nanoparticles [13]. Consequently, bleomycin saccharide glycoclusters could also be used in the delivery of oligonucleotides.

Molecular spherical nucleic acids (MSNAs) [14–22] and other dendritic nucleic acid structures [23–25] may exhibit increased cellular uptake compared to linear oligonucleotides via Scavenger A-receptor-mediated endocytosis [26, 27], improved circulation time in vivo [16, 28] and resistance to nuclease degradation [29, 30]. The exact behavior is dependent on the size, surface chemistry, and surface density of the MSNAs [28, 31–33], as well as plasma protein binding to their surface [34, 35]. Due to the multivalent nature of these nanoparticular formulations, they may offer optimal scaffolds for carbohydrate-mediated delivery. Combining glycocluster-conjugated oligonucleotides with MSNAs results in highly multivalent carbohydrate decorated structures that are reminiscent of recent C_{60}-fullerene-derived "glyco-superballs", which have found use as anti-viral agents [36, 37] and glycosidase inhibitors [38, 39]. This decoration could hide the negatively charged oligonucleotide content while simultaneously enhancing the effect of the surface ligands [17, 18, 40]. Since surface chemistry plays a major role in the protein corona of nanoparticles [34, 41, 42], it is likely that the surface decoration of MSNAs may also change their protein binding. Our previous studies have shown that surface decoration with chondroitin sulfates [18], folate [22] and Trastuzumab [14] can be used to adjust the biodistribution and cellular uptake of MSNAs.

Recently, we synthesized tripodal bleomycin saccharide (α/β-bleomycin disaccharide and carbamoyl mannose) conjugates of a splice-witching oligonucleotide (AON_{ARV7}) and hybridized these conjugates with a 12-arm C_{60}-derived MSNA consisting of complementary 2'-deoxyoligoribonucleotide sequences (Table 1) [17]. Hybridization-mediated MSNAs with 36 carbohydrate units on their surface were obtained (Scheme 1A). In this study, we optimized the synthesis of the oligonucleotide conjugates (**ON2-ON4**, Scheme 1A, Scheme S1), based on strain-promoted alkyne-nitrone cycloaddition (SPANC), and provided further characterization of the MSNAs (**MSNA1-4**), including their homogeneity/molecular weight estimation by size-exclusion chromatography equipped with multi-angle light scattering detector (SEC-MALS). Steady-state and time-resolved fluorescence techniques were used to study the effect of the sugar-moieties on the spectroscopic properties of the AF488-labeled oligonucleotide, and the formation of the MSNA was analyzed using the cooperative binding model. Cellular uptake of the conjugates (**ON1-ON4** and **MSNA1-4**) was studied in 22Rv1 and PC3 cell-lines in three different media (serum-free (SF), human serum (HS), fetal bovine serum (FBS)), using flow cytometry and fluorescence-lifetime imaging microscopy (FLIM).

2 Materials and methods

2.1 Optimized synthesis of oligonucleotide conjugates (ON2-ON4)

Nitrone-modified glycoclusters **4–6S** and dibenzocyclooctyne (DBCO)-modified oligonucleotide **ON1S** (cf. supporting information) were synthesized as previously described [17]. A multistep synthesis is required for **4–6S**, which makes them expensive starting materials. Therefore, an excess (1.5 equiv.) of **ON1S** (which can be readily synthesized by an automated synthesizer using commercially available building blocks) was used for the SPANC conjugation. Each of the glycoclusters (**4S**, **5S** or **6S**, 0.1 µmol) and **ON1S** (1.5 equiv.) were dissolved in a small amount of water (25 µL). The reaction mixtures were incubated overnight at room temperature, and the obtained oligonucleotide-glycoconjugates **ON2S-ON4S** were purified by reversed-phase high performance liquid chromatography (RP HPLC, see profiles of crude product mixtures: A-C and profiles after purification: D-F, Figure S1). The authenticity of the intermediate products (**ON2S-ON4S**) was verified by electrospray ionization time-of-flight mass spectrometry (MS, ESI-TOF). The product fractions were evaporated to dryness and the residues were dissolved in a freshly prepared mixture of dimethyl sulfoxide (DMSO, 25 µL), *N*, *N*-diisopropylethylamine (DIEA, 0.2 µmol) and AF488 *N*-hydroxysuccinimide ester (0.5 µmol). The reaction mixtures were incubated overnight at room temperature, and

Table 1 The studied MSNAs, the oligonucleotides used in hybridization and the carbohydrates on the conjugates

MSNA	Oligonucleotide	Carbohydrate
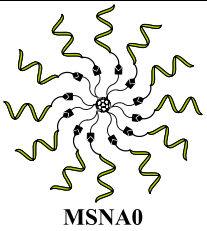 **MSNA0**	**n/a**	**n/a**
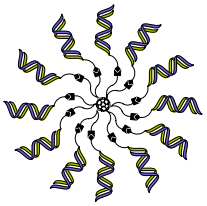 **MSNA1**	 **ON1**	**n/a**
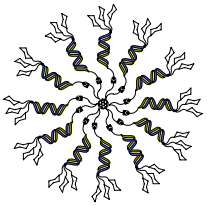 **MSNA2**	 **ON2**	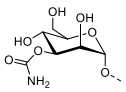 carbamoyl mannose
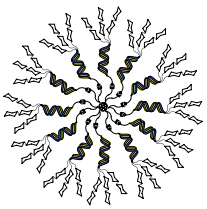 **MSNA3** **MSNA4**	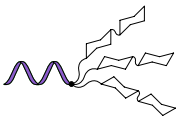 **ON3** **ON4**	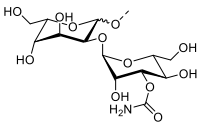 **ON3**, **MSNA3:** α-bleomycin disaccharide **ON4**, **MSNA4:** β-bleomycin disaccharide

the obtained oligonucleotide-glycoconjugates **ON2-4** were purified by RP HPLC (see profiles of crude product mixtures: G-I and profiles after purification: J-L, Figure S1). The authenticity of the products (**ON2-4**) was verified by MS (ESI-TOF). **ON2**, **ON3** and **ON4** were obtained in 33%, 19% and 15% overall yields, respectively (based on AF488-specific UV-absorbance at 497 nm).

2.2 SEC-MALS analysis

SEC-MALS analysis of the MSNAs was performed using an Äkta Pure 25 M1 HPLC-system equipped with a Wyatt miniDAWN TREOS II MALS-detector and a Wyatt Optilab T-rEX refractive index (RI) detector. A Superdex 200 Increase 10/300 GL column was used with a flow rate of 0.75 ml/min and 150 mM sodium phosphate (pH7.0) as the mobile phase. For each run, 20–40 µg of MSNA in 500 µL of the mobile phase, with 0.1 M NaCl added, was injected. A 30 min run time was used. The molecular weight was extracted from the major fraction using an average refractive index increment (dn/dc) of 0.1703 mL/g.

2.3 Absorption and fluorescence measurements

Absorption spectra of the solutions were recorded with Shimadzu UV3600 spectrophotometer (Japan) and the fluorescence spectra with FLS-1000 photoluminescence spectrometer (Edinburgh Instruments, U.K.) with 470 nm as the excitation wavelength. The fluorescence spectra were corrected according to the wavelength sensitivity of the detector and the excitation source intensity. Time-resolved fluorescence was measured using a time-correlated single photon counting (TCSPC) system (PicoQuant GmBH, Chaussee, Germany) consisting of a PicoHarp 300 controller and a PDL 800-B driver. The samples were excited with the pulsed diode laser head LDH-P-C-485 at 483 nm at a time resolution of 130 ps. The signals were detected with a microchannel plate photomultiplier tube (Hamamatsu

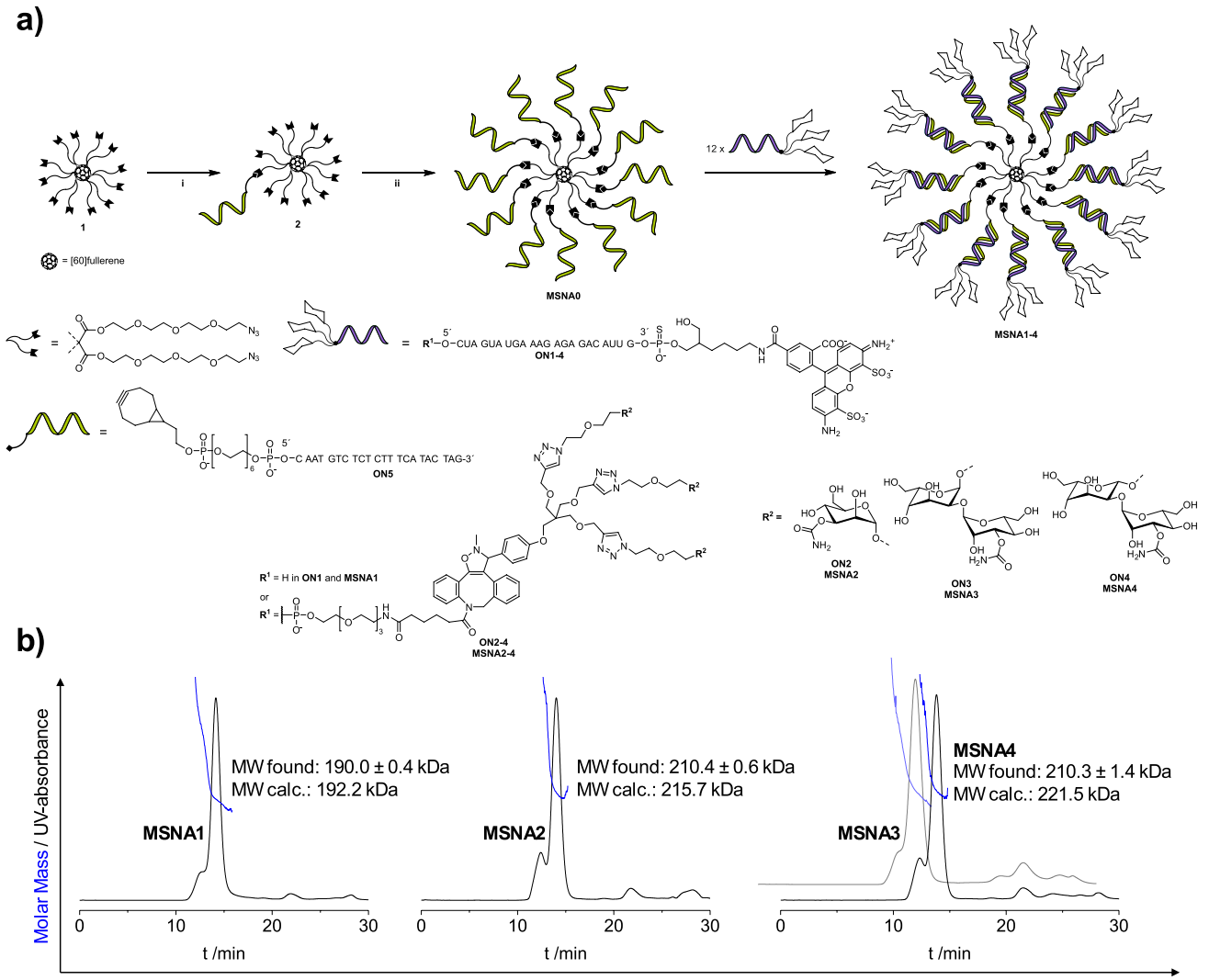

Scheme 1 **a** Synthesis of the MSNAs. **ON1-4** are 2′-OMe ribonucleotides with a phosphorothioate backbone, except for the single phosphodiester bond at the 5′-end. **ON5** is a 2′-deoxyribonucleotide with a phosphate backbone. Conditions: (i) 0.3 equiv. **ON5** in DMSO/water (9:1, *v*:*v*), (ii) 1.2 equiv./branch **ON5** in 1.5 M NaCl (aq.) **b** SEC-MALS analyses of **MSNAs1-4**

R2809U). The influence of the scattered excitation light was reduced with a cutoff filter (transmission > 490 nm) in front of the monitoring monochromator. Fluorescence decays were monitored at 520 nm. The instrumental response function (IRF) was measured separately, and the decays were deconvoluted and fitted by applying the iterative least-squares method to the sum of 1–2 exponents (Eq. 1).

$$I(t) = \sum\nolimits_i a_i e^{-t/\tau_i} \quad (1)$$

In this Eq. 1, τ_i is the global lifetime and a_i is the local amplitude (pre-exponential factor). The amplitude averaged lifetimes $\langle\tau\rangle$ were calculated using Eq. 2.

$$\langle\tau\rangle_A = \sum_i a_i\tau_i / \sum_i a_i \quad (2)$$

2.4 Cellular uptake studies for microscopy

2.4.1 Cell culture

PC3 (European Collection of Authenticated Cell Cultures, UK) and 22Rv1 (American Type Culture Collection, USA) cells were cultured in RPMI-1640 medium with L-glutamine supplemented with 1% (v/v) penicillin-streptomycin and with 10% (v/v) of either fetal bovine serum (FBS), human serum (Merck, Espoo, Finland) or without serum.

2.4.2 Widefield microscopy

For all cellular uptake studies, stock solutions of the MSNAs and oligonucleotides (1 µM) were prepared in 1 × PBS (phosphate buffered saline), which were then diluted into the media used for the studies. Uptake studies of **ON1−4** and the corresponding **MSNAs1−4** (10 nM) were carried out with PC3 and 22Rv1 cells. Data were compared to untreated PC3 and 22Rv1 cells in matching serum conditions. Uptake studies were carried out in serum-free medium as reported previously [17]. Either 86,000 cells/cm^2 PC3 or 107,500 cells/cm^2 22Rv1 cells were seeded in 8-well chamber slides in standard tissue culture conditions for 24 ± 2 hours before experimentation. Cells were then incubated with **ON1–4** or **MSNA1−4** for 4 h, after which the cells were washed with 1 × PBS- and fixed with 4% (w/v) paraformaldehyde for 15 min and stained with ProLong Diamond Antifade Mountant with DAPI (4′,6-diamidino-2-phenylindole) and sealed with a coverslip. Widefield microscopy was performed within 2 weeks of fixation. Fixed samples were imaged with a Nikon Eclipse Ti2-widefield microscope. Microscope settings were consistent throughout all experiments with each cell line. Scale bars in each image are 20 µm. Images were edited by enhancing image contrast and brightness with Fiji (10.1038/nmeth.2019) [43].

2.4.3 FLIM imaging

Cell samples were prepared 1–2 days prior to FLIM imaging. In an 8-well plate 20 000 cells/well were seeded. For 22Rv1 cells the well plates were coated with Fibronectin. For PC3 cells the medium was changed to Fluorobrite + 10% FBS 2 h before the imaging, whereas for 22Rv1 cells RPMI medium without phenol red was used. 50 µl of the MSNA sample was added into the wells at the microscope stage directly before imaging of the first time points (several minutes after the addition) followed by further imaging for 7 h. A single cell was imaged every 2 h until the end of the experiment or until the cell detached. As the aim of the study was to monitor the trafficking of MSNAs in the cells, the excess of the label was not washed out prior the FLIM measurements in contrast to conventional sample preparation for confocal microscopy. This was possible as the signal intensity in the cell area was incomparably high regarding the background intensity in the medium. Moreover, the area inside the cell was selected as the region of interest (ROI) for further analysis allowing to exclude the effect of the background.

Fluorescence lifetime images were acquired using a fluorescence lifetime microscope MicroTime-200 (PicoQuant, Germany) coupled to the inverted microscope Olympus IX-71 (Olympus, Japan). Imaging with a 100 × oil objective having NA 1.4 enabled a minimum spatial resolution of 300 nm and a maximum scan area of 80 µm × 80 µm. The pulsed laser diode LDH-P-C483 (PicoQuant, Germany) emitting at 483 nm (time resolution 120 ps) was used for excitation and the emission was monitored using 510 nm long pass filter. During imaging the living cells were kept at 37 °C and at 5% CO_2 using an objective heater (Bioscience Tools, California, USA, TC-1–1005 Temperature Controller) and a custom-made incubator. The SymPhoTime 64 software was used to calculate the lifetime map images. The colors of the FLIM images present the mean arrival time of the emitted photons after the excitation pulse (τ_{fast}) in each pixel. To gain more information on the lifetime changes, fluorescence decays were extracted from the ROIs. The decay curves were fitted by applying iterative least-squares method to the sum of exponents in the Eq. 1 and the intensity averaged fluorescence lifetimes were calculated with Eq. 3:

$$\langle \tau \rangle_I = \sum_i a_i \tau_i^2 / \sum_i a_i \tau_i \tag{3}$$

2.5 Enzymatic stability assay

The MSNAs were diluted into 10mM tris-HCl (pH 7.5 with 2.5 mM $MgCl_2$ and 0.1 mM $CaCl_2$). The MSNAs (10 µL, c(MSNA) = 0.05 µM) were incubated at 37 °C with deoxyribonuclease (DNase) I (1 U/nmol and 5 U/nmol effective oligonucleotide content). After 24 h, 5 µL samples from the reactions were taken and added into 3 µL of Novex Hi-Density TBE (tris, borate, ethylenediaminetetraacetic acid) Sample Buffer (Invitrogen) on ice. 6.5 µL of each sample was loaded onto a 6% TBE polyacrylamide gel which was electrophoresed at a constant 100 V for 1 h. After completion, the gel was stained by SYBR Gold Nucleic Acid Stain (Invitrogen) and imaged.

2.6 Quantitative cell uptake and flow cytometry

Quantitative uptake studies of **ON1−4** and the corresponding **MSNAs1–4** (both 2.5 nM) were carried out with 22Rv1 cells, with untreated cells as control. Cells were seeded into either 24-well (105,300 cells/cm^2) or 6-well plates (57,700 cells/cm^2) for flow cytometry. Cells were incubated under standard tissue culture conditions with either **ON1−4** or **MSNAs1–4** for 4 h. After quantitative cell uptake, cells were washed with 1 × PBS- and detached with 50 µL TrypLE Express. Cells were then resuspended in cold 1 × PBS- and pelleted by centrifugation (200 × g, 5 min). The pellets were washed with 1 x PBS- and the cells were resuspended in 1 mL 1 × PBS- for FBS and serum-free cells and in 600 µL for cells in HS. The mean fluorescence intensity (MFI)

from MSNAs internalized by cells was detected using BD LSR Fortessa flow cytometry instrument (BD Biosciences, NJ, USA) with solid state diode blue laser (488 nm, 50 mW) and 530/30 bandpass filter. FlowJo v10 software was utilized for the data analysis, and the MFI values were subsequently normalized to the control group (untreated cells with the same growth media condition) resulting in an arbitrary unit of 1 ($n=3$). To eliminate the fluorescence intensity variations between the samples due to glycodecoration, the acquired arbitrary units were further normalized by dividing their positive deviation from the control by the relative fluorescence efficiencies of the structures acquired by fluorescence measurements (see correction factors for flow cytometry in supporting information).

3 Results and discussion

3.1 Synthesis

Oligonucleotide conjugates **ON1-ON4** and **MSNA0** were synthesized following previously published protocols (Scheme 1A) [17]. Strain-promoted alkyne-nitrone cycloaddition (SPANC) [44] between nitrone-modified bleomycin saccharide derivatives and a dibenzocyclooctyne-modified oligonucleotide, followed by labelling with Alexa Fluor (AF488) *N*-hydroxysuccinimide ester, and including two RP HPLC purifications, gave the oligonucleotide conjugates **ON2-ON4** in 33, 19 and 15% overall yield, respectively (Scheme S1). The hybridization-mediated **MSNAs 1–4** were assembled by mixing **MSNA0** with the corresponding oligonucleotides in a medium (specified later for each use case). The homogeneity and molecular weight of the MSNAs were estimated by SEC-MALS (Scheme 1B). The samples were prepared in phosphate buffer (pH 7.0) with added NaCl (0.1 M) using 12 equivalents of the complementary oligonucleotide (**ON1-4**). The chromatograms show a major fraction corresponding to the MSNA and a smaller, faster eluting fraction of high molecular weight substance, likely caused by aggregation. Molecular weights of 190 kDa (**MSNA1**), 210 kDa (**MSNA2**) and 210 kDa (**MSNA3/4**) were extracted from MALS of the major fraction (using a dn/dc of 0.1703 ml g^{-1}). The observed molecular masses matched calculated molecular masses of **MSNAs1-2** relatively well (calc MW: 192 and 215 kDa, respectively) and ca. 5% mass deviation was observed in the case of **MSNA3-4** (calc MW: 222 kDa). In our previous study [17] molecular mass of **MSNA0** was verified by MS, and its hybridization with **ON1-ON4** was studied by polyacrylamide gel electrophoresis (PAGE), DLS and melting temperature studies, all of which indicated nearly identical behavior for **MSNAs1-4**.

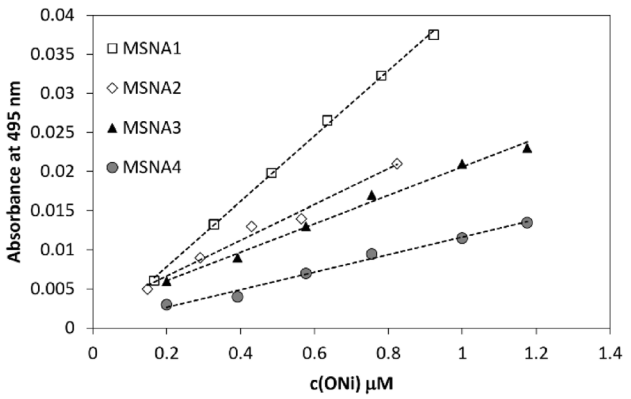

Fig. 1 Absorbance at the maximum wavelength as a function of oligonucleotide concentration during hybridization with oligonucleotide-MSNA ratios 2–12

3.2 Hybridization of MSNA0

The hybridization between **MSNA0** and the AF488-labeled oligonucleotides **ON1-4** was studied by absorption and fluorescence spectroscopy. The presence of sugar-moieties in the oligonucleotides **ON2-4** decreased the absorbance of AF488 to about half of that in the absence of the sugar-moieties in **ON1** (Figure S3). Thus, some interaction between AF488 and the sugar moieties takes place already in the ground state. To observe the effect of sugar-moieties on fluorescence intensity, the fluorescence efficiencies φ_{eff} of the oligonucleotides were calculated as

$$\varphi_{eff} = \frac{I_{FL,tot}}{A_{\lambda_{ex}}} \qquad (4)$$

where $I_{FL,tot}$ is the total fluorescence, i.e. the area under the fluorescence spectrum, and $A_{\lambda_{ex}}$ is the absorbance at the excitation wavelength. Comparing the obtained values to that of **ON1**, the fluorescence efficiency is only somewhat smaller for the sugar decorated oligonucleotides (Table S1).

To study the formation of **MSNAs 1–4** different concentrations of oligonucleotides were added to **MSNA0** solution corresponding to **ONi**:**MSNA0** ratios 2, 4, 6, 8, 10, and 12. The changes in the AF488 absorbances as a function of the oligonucleotide concentration are plotted in Fig. 1 and the spectra are shown in Figure S4. The absorbance increases linearly for all MSNAs, but the increase is much shallower for the sugar decorated oligonucleotides than for **ON1**. Thus, the decrease in the molar absorption coefficient induced by the presence of sugar-moieties is retained during the hybridization.

The fluorescence intensity increased during complexation (Figure S5) partly due to the increase in the absorbance. The φ_{eff}-values in the presence of **MSNA0** were normalized with the φ_{eff}-values in the absence of **MSNA0** and the results are shown in Fig. 2 as a function of

the oligonucleotide concentration. For **MSNA1** no change in the φ_{eff}^{norm} is observed at the lowest concentration corresponding to the oligonucleotide-MSNA ratio 2. However, for all the sugar decorated oligonucleotides the fluorescence is strongly quenched already at this ratio. For **MSNA1** the fluorescence efficiency decreases with increasing **ON1** concentration up to oligonucleotide-MSNA ratio 12, whereas for the sugar-decorated MSNAs it first increases. For **ON2**, the φ_{eff}^{norm} increases slightly for the oligonucleotide-MSNA ratio 4, but stays nearly constant after that. For **ON3** and **ON4**, φ_{eff}^{norm} increases with increasing oligonucleotide concentration until oligonucleotide-MSNA ratio 8. At this ratio, the curve of **ON3** levels off whereas the efficiency for **ON4** starts to decrease. Thus, the sugar moieties clearly have an effect on the formation of the MSNA-complexes. While for **ON1** a full complex with all the 12 arms of **MSNA0** bound with the complementary oligonucleotide is formed, it seems that for the other oligonucleotides the complexation is not proceeding as smoothly. The ground state interaction between the AF488 and the sugar moieties could hinder the complexation since during the complexation these interactions should break. This could induce the initial increase in the relative fluorescence efficiency.

For the sugar derivatives, the absorption spectra are noisy and thus, although the steady-state data are good for qualitative analysis, no quantitative estimations can be drawn from it. Since fluorescence lifetimes do not depend on dye concentration, further analysis was done from the time-resolved data. For **ON2-4** the fluorescence decay curves are one-exponential, whereas for **ON1** and all the MSNAs they are two-exponential (Figure S6). Thus, amplitude averaged fluorescence lifetime ⟨τ⟩ (Table S2) was utilized to describe the overall change in the fluorescence decays. ⟨τ⟩ decreased during complexation for all oligonucleotides. For **ON1** and **ON2**, the decrease was due to the increase in the proportion of the short-living component, whereas for **ON3−4**, both the lifetime and the proportion of the short-living component changed during complexation.

Recently, we determined the binding constants for MSNAs using an independent binding model [17]. The independent binding model does not consider the simultaneous or subsequent binding of other oligonucleotides at unoccupied complementary branches of the MSNA. However, the complex behavior of the fluorescence efficiencies (Fig. 2) implies that the complexation does not happen this way. Thus, we decided to use the cooperative binding model [45] to analyze our data. In this model the binding of a ligand to a site on a target molecule can influence the binding of other ligands to other unoccupied sites on the same target. For positive cooperativity, the binding of first ligand makes it easier for the next one to be bound whereas for negative cooperativity each succeeding ligand is bound

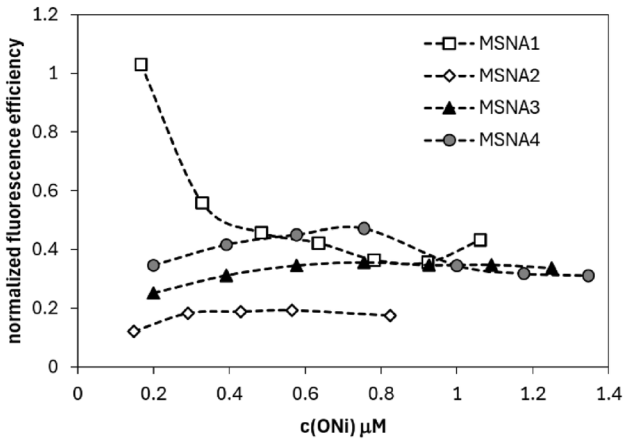

Fig. 2 Normalized fluorescence efficiencies as a function of oligonucleotide concentration corresponding to oligonucleotide-MSNA ratios from 2 − 14 (12 for **ON2**)

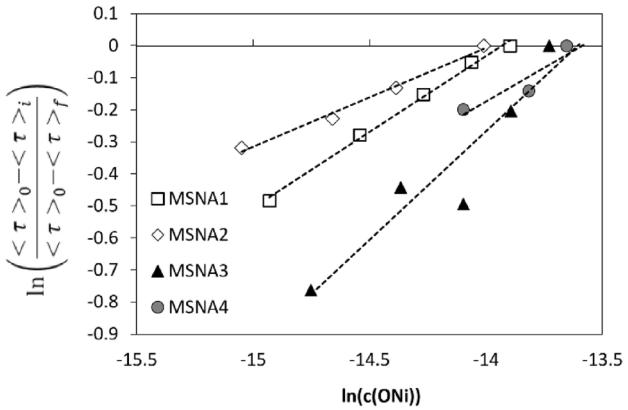

Fig. 3 Hill plots for the MSNAs, i.e. $\ln\left(\frac{<\tau>_0-<\tau>_i}{<\tau>_0-<\tau>_f}\right)$ as a function of $\ln[ON]$

less strongly than the previous one. The Hill plot model for a ligand binding to multisubunit [46–49] substrate was used to estimate the cooperativity of our systems through Eq. 5:

$$\ln\left(\frac{<\tau>_0-<\tau>_i}{<\tau>_0-<\tau>_f}\right)=\alpha\ln[ON]+\alpha\ln K \qquad (5)$$

where $<\tau>_0$ is the average fluorescence lifetime in the absence of MSNA, $<\tau>_i$ is the average fluorescence lifetime in the presence of MSNA, $<\tau>_f$ is the average fluorescence lifetime of the complex at ratio oligonucleotide-MSNA ratio 12, α is the experimental Hill′s coefficient defining the degree of cooperativity of the binding and K_c is the binding constant. The Hill′s coefficient α varies from independent value of $\alpha=1$ to $\alpha>1$ for positive cooperativity and $\alpha<1$ for negative cooperativity. The Hill plots for the present systems are presented in Fig. 3 and the results are listed in Table 2.

Table 2 Association constants K_{co} and Hill´s coefficients α for **MSNA1-4** complexes from the cooperative model at oligonucleotide-MSNA ratios higher than 4 and association constants from independent binding model K_{in} at oligonucleotide-MSNA ratios 2–4

MSNA1	ON: MSNA ratio	K_{co}	α	K_{in} (2–4)[a]
	4–12	1.12×10^6	0.4732	9.17×10^7
MSNA2	4–12	1.17×10^6	0.3087	2.08×10^6
MSNA3	4–12	8.11×10^5	0.6772	6.67×10^8
MSNA4	8–12	7.95×10^5	0.4214	4.55×10^8

[a] determined from equation $\frac{1}{<\tau>} = 1 + \frac{1}{K[ONi]}$

All MSNAs show negative cooperativity with α varying between 0.3 and 0.7. The binding constants are of the same magnitude for all MSNAs but are slightly lower for **MSNA3-4** than for **MSNA1-2**. The linear dependencies were observed at ratios 4–12 and only at 8–12 for **MSNA4**. At lower ratios the binding is independent leading to much higher binding constants, K_{in} in Table 2, for all MSNAs but **MSNA2**. The complex formation is most efficient at low oligonucleotide-MSNA ratios, when there is plenty of free arms and no need to bind on an arm adjacent to an already hybridized one. Once the complexation proceeds, the already bound oligonucleotides hinder the binding of further oligonucleotides to the MSNA. Surprisingly the initial binding seems to be strongest for the bleomycin-derivatives (**MSNA3-4)** and weakest for the carbamoylmannose-derivative (**MSNA2)**. Also, the negative cooperativity is lowest, α is closest to 1, for **MSNA3** indicating that the full complex is formed more easily with this system. The weakest complex formation seems to be for the **MSNA2** and no large differences are observed between **MSNA1** and **MSNA4**. As a summary, the presence of the sugar groups clearly influences the spectral properties of AF488 and do seem to hamper the formation of the MSNA complex. All the MSNAs show negative cooperativity in the binding and the complexation seems to be complete at oligonucleotide-MSNA ratio 12.

3.3 Cellular uptake of MSNAs

The uptake of the conjugates was evaluated by wide-field microscopy (WF) and FLIM (Fig. 4) in 22Rv1 and PC3 cell-lines using 10 nM sample concentration. In both cell types, MSNAs are taken up relatively effectively, with PC3 cells showing a more diffuse cytoplasmic distribution, while in 22Rv1 cells signal appears as bright vesicular spots, indicating possible endosomal entrapment upon internalization.

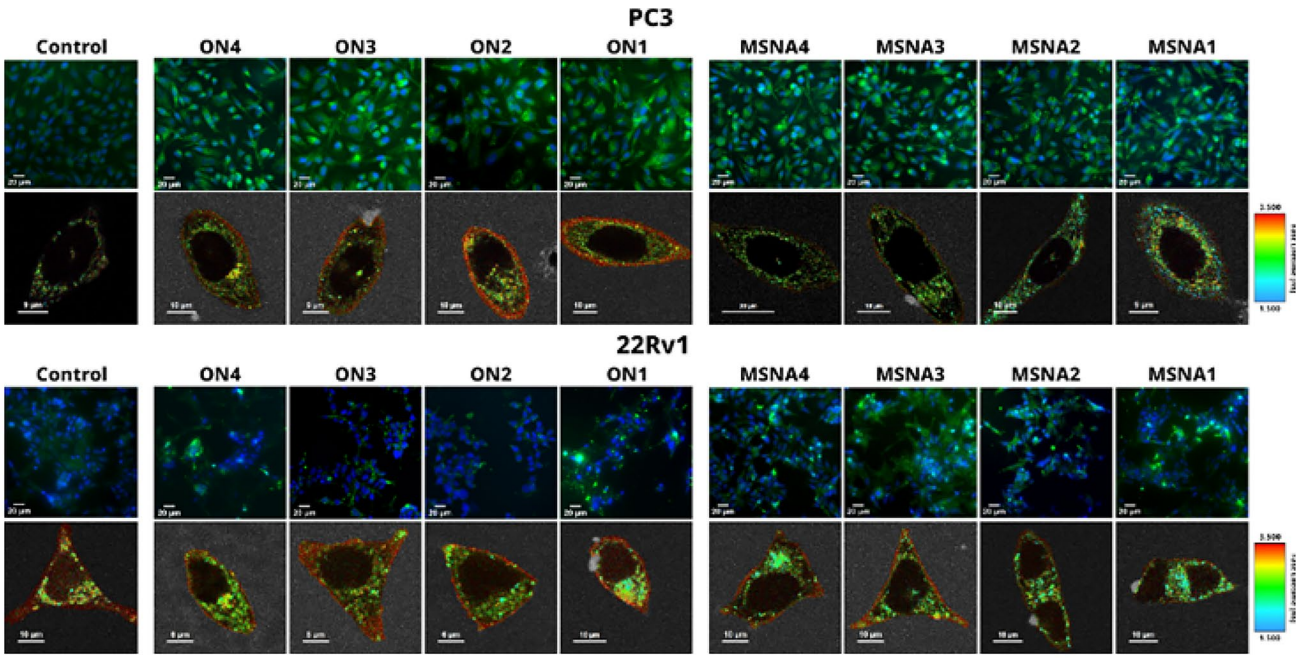

Fig. 4 FLIM and wide-field fluorescent microscopy (WF) images of PC3 (top) and 22rv1 (bottom) cells at 5 h after addition of MSNA-complexes to the cell culture medium. The final concentration of the MSNA-complexes in the cell culture medium was 10 nM in all cases. For each cell-line, upper row has WF images and the lower row FLIM images. The control images on the left show the autofluorescence of the cells. In the WF images, DAPI fluorescence is shown in blue and AF488 in green. In the FLIM images, the color of each pixel correlates with the average fluorescence lifetime in the corresponding spatial location, the scale bars are given on the right. The excitation wavelength was 483 nm, the fluorescence was monitored between 510–800 nm and the time-resolution of the system was 130 ps. The gray areas in some of the FLIM images are not attached to the cells but are MSNA-complex aggregates floating in the medium and have thus been omitted from the ROI. For **MSNAs3-4** the strong fluorescence of the MSNA-complexes in the medium is visible and thus the background in these images is less dark

The uptake of the MSNAs did not affect the cell morphology or density/confluency of PC3 cells.

In FLIM images of PC3 cells, the autofluorescence of the cells gives a weak signal with an average lifetime of 2.3 ns. 5 h after addition of MSNAs into the cell culture medium, the uptake of non-glycoconjugated **MSNA1** is clearly visible as blue spots and more uniform green color in the cell. For the glycoconjugated MSNAs the uptake is more difficult to see, since there are very little changes in the fluorescence lifetime compared to that of autofluorescence. However, for **MSNA2** some blue and yellow spots are visible and for **MSNA3** a weak fluorescence with a longer lifetime is observed on the cell membrane. These findings are more pronounced when the images at different time points are compared with each other (Figures S7-S10). The changes clearly differ from those observed for free oligonucleotides: the accumulation of the oligonucleotides on the outer cell membrane is observed as red borders on the cells with longer lifetimes close to 3 ns. This signal is observed already at 1 h after addition of the oligonucleotide to the cell culture medium. The 22Rv1 cells have more intense autofluorescence with average lifetime of 2.5 ns and the MSNA uptake is now observed as decrease in the lifetime i.e. increased amount of blue and green colors. This is opposite to that observed for free oligonucleotides with 22Rv1 cells: again, the free oligonucleotides gather to the outer cell membrane and have a longer lifetime than the MSNAs.

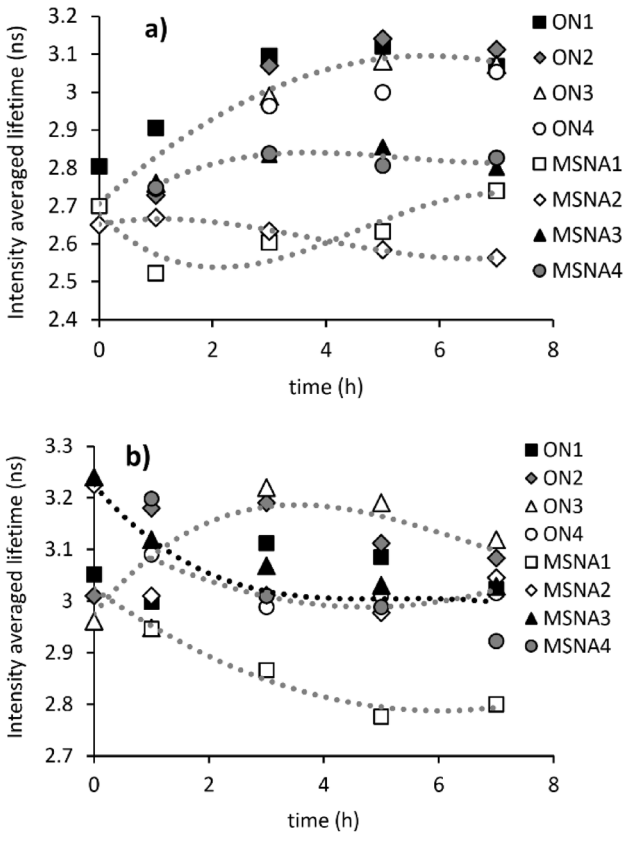

Fig. 5 The intensity averaged fluorescence lifetimes as a function of time after adding oligonucleotides and MSNAs into the cell culture medium of (a) PC3 and (b) 22Rv1 cells. The trend lines are there only to guide the eye

To gain more information on the lifetime changes, the area inside the cell was selected as the region of interest (ROI) and fluorescence decays were extracted from them. The intensity weighted average fluorescence lifetimes, $< \tau >_I$, were calculated from the decays (Eq. 3) and are plotted as a function of the measuring time in Fig. 5. Please note that the $< \tau >_I$-values are not equal to the lifetimes observed in the FLIM images, but the changes in $< \tau >_I$ -values correspond to the changes in the FLIM image lifetimes. In PC3 cells $< \tau >_I$ increases for all oligonucleotides from about 2.7 ns in the absence of oligonucleotides to about 3.1 ns at 5 h after addition of oligonucleotides to the cell culture medium. In the presence of MSNA-complexes, no red border is observed for PC3 cells. For **MSNA1**, the $< \tau >_I$ first decreases to 2.52 ns and then starts to increase returning to back to 2.7 ns at 7 h after addition. In FLIM images (Figure S8) faint blue spots are observed in the cell membrane as the MSNA complexes are taken up by the cell. In time, some of these spots turn to green and further on to yellow, which could indicate that the MSNA-complexes are "opening" explaining the change in $< \tau >_I$. For **MSNA2**, $< \tau >_I$ decreases with time and blue spots are visible on the FLIM images indicating that some MSNAs are taken in but stay intact during the measurements. For **MSNA3** and **MSNA4** $< \tau >_I$ stays nearly constant during the measurements and no conclusions on the uptake and the subsequent fate of the MSNAs can be made.

The changes in $< \tau >_I$ are smaller for 22Rv1 cells than for PC3 cells, which can be partly due to the higher autofluorescence observed for 22Rv1 cells. In 22Rv1 cells, $< \tau >_I$ increases for **ON1–3** from about 3.1 ns in the absence of oligonucleotides to about 3.2 ns at 3 h after addition and then it decreases to 3.05 ns. For **ON4**, $< \tau >_I$ decreases a little between 1 and 3 h after addition and stays constant after that. In the presence of MSNA-complexes the $< \tau >_I$ decreases by about 0.2 ns during 5 h after addition indicating that some MSNAs are taken in but stay intact during the measurements.

Following FLIM and WF, we evaluated the effect of carbohydrate decoration and the effect of the medium on the cellular uptake of the conjugates and MSNAs using flow cytometry. Since both the carbohydrates and the MSNA formulation quenched the fluorescence to a varying degree, this was taken into account in the analysis of the flow cytometry results (Fig. 6, Table S3). The cellular uptake of the conjugates in different media was then evaluated in the 22Rv1 cell-line using a 2.5 nM sample concentration.

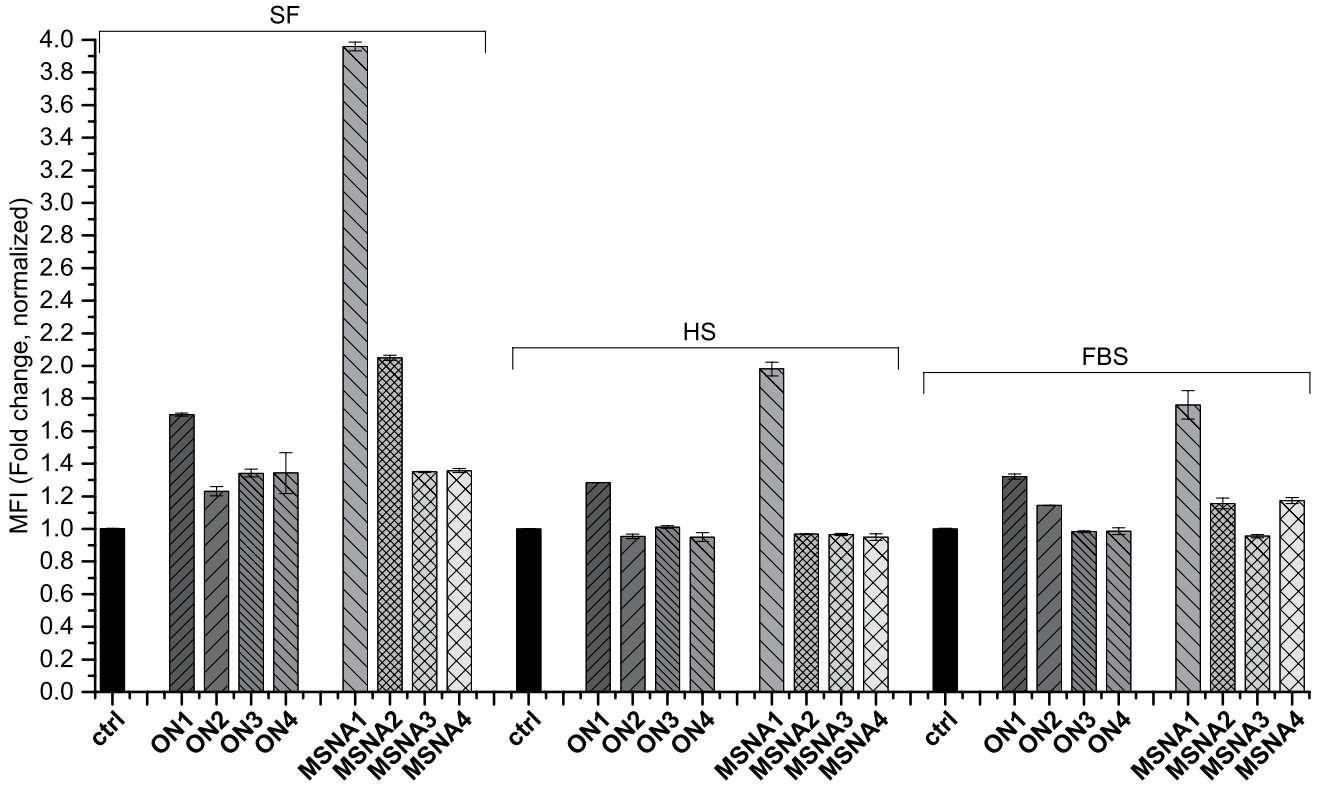

Fig. 6 Cellular uptake of the conjugates in 22Rv1 cell-line evaluated by flow cytometry. Media are as follows: serum-free (SF), human serum (HS), fetal bovine serum (FBS). The positive deviation from control is normalized according to the observed fluorescence quenching assuming that the MSNAs are fully hybridized and intact

Due to the potential dissociation of the MSNAs in cells, and its effect on fluorescence, accurate comparison between the MSNAs and oligonucleotides cannot be done in these experiments. It can still be observed that **MSNA1** (without sugar decoration) was taken up in each medium (serum free = SF, human serum = HS, fetal bovine serum = FBS) most efficiently, as could be inferred from the FLIM data as well. The most efficient uptake can be observed in serum-free conditions (SF). It is possible that in serum (HS and FBS) protein binding to the MSNAs inhibits the uptake, however one should also consider the markedly increased uptake in SF condition could be resulted from stress-induced endocytosis [50]. Excluding the uptake of **MSNA2** (with carbamoyl mannose decoration) in SF, the glycoconjugated structures showed marginal uptake in the given 2.5 nM concentration (cf. the uptakes in the FLIM studies, when 10 nM concentration was used). The sugar moieties seemed to interfere with the potential Scavenger A receptor-mediated uptake perceived with MSNAs (cf. **MSNA1**), and they did not show a beneficial compensating impact on the uptake under the studied concentration.

Finally, the enzymatic stability of the MSNAs was evaluated by incubating them with DNase I (1 U/nmol and 5 U/nmol of the effective oligonucleotide content) and their degradation was monitored by polyacrylamide gel electrophoresis (PAGE) (Figure S11). The MSNAs were degraded by DNase I, albeit very slowly (only partial degradation after 24 h) compared to other MSNAs on the same C_{60}-carrier [18, 22]. As expected, the full phosphorothioate backbone of the complementary oligonucleotide increased the stability. Based on the slow degradation, the primary mechanism for the release of the oligonucleotide is passive dissociation and not carrier degradation.

4 Conclusions

An optimized SPANC conjugation between nitrone-modified glycoclusters and a cyclooctyne-modified oligonucleotide yielding bleomycin saccharide-oligonucleotide conjugates has been described. The oligonucleotide-conjugates were used for the assembly of hybridization-mediated MSNAs. SEC-MALS proved a valuable tool for evaluating homogeneity and authenticity of the hybridization-mediated MSNAs (of 192, 216 and 222 kDa). Cellular uptake of the MSNAs in 22Rv1 and PC3 cell-lines was evaluated by fluorescence-lifetime imaging microscopy (FLIM), wide-field microscopy and flow cytometry. In FLIM experiments, some cellular uptake was observed in 10 nM sample concentration in both cell lines and the results were clearer in

the PC3 cell line whose autofluorescence was weaker. In PC3 cells some indication that the non-conjugated **MSNA1** dissociates following uptake was observed, whereas no such observation was made for the glyco-conjugated **MSNA2–4**. In flow cytometry data, it was obvious that the carbohydrate conjugation of the structures interfered with the uptake. Minor differences between the different carbohydrates were observed. Out of the carbohydrate-modified MSNAs, **MSNA2** (with carbamoyl mannose decoration) was taken up marginally better than the others, which was in agreement with our preliminary observation [17]. It is worth mentioning that effective oligonucleotide concentration is used in each case to make this comparison, i.e. 12 fold more diluted concentrations are used for MSNAs than for single oligonucleotides. In contrast to the expectation that sugars would benefit the uptake of MSNAs, it seems likely that the carbohydrates interfere with the Scavenger A-mediated endocytosis, and cannot compensate this with potential sugar-mediated delivery. While small-molecule conjugation of MSNAs may still prove to be an effective method for the delivery of oligonucleotides, it seems evident that more powerful ligands are needed to achieve a significant positive effect. It is not a coincidence that the *N*-acetylgalactosamine - asialoglycoprotein receptor recognition has emerged as an effective delivery method for oligonucleotides. The same ligand-recognition could be applied with MSNAs, but can lead to an enhanced liver targeting only. For the extrahepatic delivery, antibody-like strong binders [14] such as darpins or aptamers may be applied.

Supplementary Information The online version contains supplementary material available at https://doi.org/10.1007/s43630-026-00910-3.

Acknowledgements Wide-field fluorescence microscopy and flow cytometry was performed at the Cell Imaging and Cytometry Core, Turku Bioscience Centre (Turku, Finland), with the support of Biocenter Finland. Ester Pöyhtäri and Oliver Koivisto are greatly acknowledged for the technical support for cell culture. Financial support of the Doctoral Programme in Exact Sciences (EXACTUS), University of Turku, Finnish Cultural Foundation and Turku University Foundation are acknowledged. Academy of Finland (projects no. 311362 and 363128, flagship GeneCellNano, PREIN flagship programme), EU consortium project 'Non-Animal Platform for Nanoparticle-Based Delivery Across the Blood–Brain Barrier Interface with Vehicle Evolution'(NAP4DIVE) led by Åbo Akademi University is acknowledged. Business Finland co-innovation project "3D Cure" (575/31/2023).

Author contributions T.L., V.G. and P.V. were responsible of synthetic work and characterization of the compounds.I.K., E.Lö., E.Li., AG and EV-L were responsible of FLIM studies.A.-M.Y., E.Ö., S.S., P.P., M.Y. and J.R. were responsible of cell imaging and flow cytometry studies.T.L. and I.K. contributed equally to this work. T.L., I.K., E.V.-L. and P.V. wrote the manuscript text.All authors reviewed the manuscript.

Funding Open Access funding provided by University of Turku (including Turku University Central Hospital).

Data availability No datasets were generated or analysed during the current study.

Declarations

Conflict of interest The authors declare no competing interests.

References

1. Roberts, T. C., Langer, R., & Wood, M. J. A. (2020). Advances in oligonucleotide drug delivery. *Nature Reviews. Drug Discovery, 19*(10), 673–694. https://doi.org/10.1038/s41573-020-0075-7
2. Kumar, V., & Turnbull, W. B. (2023). Targeted delivery of oligonucleotides using multivalent protein–carbohydrate interactions. *Chemical Society Reviews, 52*(4), 1273–1287. https://doi.org/10.1039/D2CS00788F
3. Nair, J. K., Willoughby, J. L. S., Chan, A., Charisse, K., Alam, M. R., Wang, Q., Hoekstra, M., Kandasamy, P., Kelin, A. V., Milstein, S., Taneja, N., Oshea, J., Shaikh, S., Zhang, L., Van Der Sluis, R. J., Jung, M. E., Akinc, A., Hutabarat, R., Kuchimanchi, S., … Manoharan, M. (2014). Multivalent *N*-acetylgalactosamine-conjugated siRNA localizes in hepatocytes and elicits robust RNAi-mediated gene silencing. *Journal of the American Chemical Society, 136*(49), 16958–16961. https://doi.org/10.1021/ja505986a
4. Abraham, A. T., Lin, J. J., Newton, D. L., Rybak, S., & Hecht, S. M. (2003). RNA cleavage and inhibition of protein synthesis by bleomycin. *Chemistry & Biology, 10*(1), 45–52. https://doi.org/10.1016/S1074-5521(02)00306-X
5. de Wit, R., Stoter, G., Kaye, S. B., Sleijfer, D. T., Jones, W. G., ten Bokkel Huinink, W. W., Rea, L. A., Collette, L., & Sylvester, R. (1997). Importance of bleomycin in combination chemotherapy for good-prognosis testicular nonseminoma: A randomized study of the European Organization for Research and Treatment of Cancer Genitourinary Tract Cancer Cooperative Group. *Journal of Clinical Oncology, 15*(5), 1837–1843. https://doi.org/10.1200/JCO.1997.15.5.1837
6. Roy, B., & Hecht, S. M. (2014). Hairpin DNA sequences bound strongly by bleomycin exhibit enhanced double-strand cleavage. *Journal of the American Chemical Society, 136*(11), 4382–4393. https://doi.org/10.1021/ja500414a
7. Yu, Z., Schmaltz, R. M., Bozeman, T. C., Paul, R., Rishel, M. J., Tsosie, K. S., & Hecht, S. M. (2013). Selective tumor cell targeting by the disaccharide moiety of bleomycin. *Journal of the American Chemical Society, 135*(8), 2883–2886. https://doi.org/10.1021/ja311090e

8. Yu, Z., Paul, R., Bhattacharya, C., Bozeman, T. C., Rishel, M. J., & Hecht, S. M. (2015). Structural features facilitating tumor cell targeting and internalization by bleomycin and its disaccharide. *Biochemistry*, *54*(19), 3100–3109. https://doi.org/10.1021/acs.biochem.5b00277
9. Schroeder, B. R., Ghare, M. I., Bhattacharya, C., Paul, R., Yu, Z., Zaleski, P. A., Bozeman, T. C., Rishel, M. J., & Hecht, S. M. (2014). The disaccharide moiety of bleomycin facilitates uptake by cancer cells. *Journal of the American Chemical Society, 136*(39), 13641–13656. https://doi.org/10.1021/ja507255g
10. Bhattacharya, C., Yu, Z., Rishel, M. J., & Hecht, S. M. (2014). The carbamoylmannose moiety of bleomycin mediates selective tumor cell targeting. *Biochemistry, 53*(20), 3264–3266. https://doi.org/10.1021/bi500482q
11. Madathil, M. M., Bhattacharya, C., Yu, Z., Paul, R., Rishel, M. J., & Hecht, S. M. (2014). Modified bleomycin disaccharides exhibiting improved tumor cell targeting. *Biochemistry, 53*(43), 6800–6810. https://doi.org/10.1021/bi501102z
12. Chapuis, J. C., Schmaltz, R. M., Tsosie, K. S., Belohlavek, M., & Hecht, S. M. (2009). Carbohydrate dependent targeting of cancer cells by bleomycin-microbubble conjugates. *Journal of the American Chemical Society, 131*(7), 2438–2439. https://doi.org/10.1021/ja8091104
13. Yao, X., Zhu, Q., Li, C., Yuan, K., Che, R., Zhang, P., Yang, C., Lu, W., Wu, W., & Jiang, X. (2017). Carbamoylmannose enhances the tumor targeting ability of supramolecular nanoparticles formed through host–guest complexation of a pair of homopolymers. *Journal of Materials Chemistry B, 5*(4), 834–848. https://doi.org/10.1039/C6TB02863B
14. Äärelä, A., Räsänen, K., Holm, P., Salo, H., & Virta, P. (2023). Synthesis of site-specific antibody-[60]Fullerene-oligonucleotide conjugates for cellular targeting. *ACS Applied Bio Materials, 6*(8), 3189–3198. https://doi.org/10.1021/acsabm.3c00318
15. Gulumkar, V., Tähtinen, V., Ali, A., Rahkila, J., Valle-Delgado, J. J., Äärelä, A., Österberg, M., Yliperttula, M., & Virta, P. (2022). Synthesis of an azide- and tetrazine-functionalized [60]Fullerene and its controlled decoration with biomolecules. *ACS Omega, 7*(1), 1329–1336. https://doi.org/10.1021/acsomega.1c05955
16. Äärelä, A., Auchynnikava, T., Moisio, O., Liljenbäck, H., Andriana, P., Iqbal, I., Lehtimäki, J., Rajander, J., Salo, H., Roivainen, A., Airaksinen, A. J., & Virta, P. (2023). In vivo imaging of [60]Fullerene-based molecular spherical nucleic acids by positron emission tomography. *Molecular Pharmaceutics, 20*(10), 5043–5051. https://doi.org/10.1021/acs.molpharmaceut.3c00370
17. Tähtinen, V., Gulumkar, V., Maity, S. K., Yliperttula, A. M., Siekkinen, S., Laine, T., Lisitsyna, E., Haapalehto, I., Viitala, T., Vuorimaa-Laukkanen, E., Yliperttula, M., & Virta, P. (2022). Assembly of Bleomycin saccharide-decorated spherical nucleic acids. *Bioconjugate Chemistry, 33*(1), 206–218. https://doi.org/10.1021/acs.bioconjchem.1c00539
18. Laine, T., Deshpande, P., Tähtinen, V., Coffey, E. T., & Virta, P. (2025). Chondroitin Sulfate-coated heteroduplex-molecular spherical nucleic acids. *ChemBioChem, 26*(6), Article e202400908. https://doi.org/10.1002/cbic.202400908
19. Li, H., Zhang, B., Lu, X., Tan, X., Jia, F., Xiao, Y., Cheng, Z., Li, Y., Silva, D. O., Schrekker, H. S., Zhang, K., & Mirkin, C. A. (2018). Molecular spherical nucleic acids. *Proceedings of the National Academy of Sciences of the United States of America, 115*(17), 4340–4344. https://doi.org/10.1073/pnas.1801836115
20. Zhang, B., Bai, S., Chao, X., Wu, T., Chen, Z., Cheng, Z., Xiao, Y., Zhang, K., & Bai, Y. (2021). Molecularly pure miktoarm spherical nucleic acids: Preparation and usage as a scaffold for abiotic intracellular catalysis. *Chemical Science, 12*(48), 15843–15848. https://doi.org/10.1039/D1SC04833C
21. Gulumkar, V., Äärelä, A., Moisio, O., Rahkila, J., Tähtinen, V., Leimu, L., Korsoff, N., Korhonen, H., Poijärvi-Virta, P., Mikkola, S., Nesati, V., Vuorimaa-Laukkanen, E., Viitala, T., Yliperttula, M., Roivainen, A., & Virta, P. (2021). Controlled monofunctionalization of molecular spherical nucleic acids on a Buckminster Fullerene core. *Bioconjugate Chemistry, 32*(6), 1130–1138. https://doi.org/10.1021/acs.bioconjchem.1c00187
22. Auchynnikava, T., Äärelä, A., Moisio, O., Liljenbäck, H., Andriana, P., Iqbal, I., Laine, T., Palani, S., Lehtimäki, J., Rajander, J., Salo, H., Airaksinen, A. J., Virta, P., & Roivainen, A. (2025). Biological evaluation of molecular spherical nucleic acids: Targeting tumors via a hybridization-based folate decoration. *ACS Omega, 10*(6), 6003–6014. https://doi.org/10.1021/acsomega.4c10047
23. Distler, M. E., Teplensky, M. H., Bujold, K. E., Kusmierz, C. D., Evangelopoulos, M., & Mirkin, C. A. (2021). DNA dendrons as agents for intracellular delivery. *Journal of the American Chemical Society, 143*(34), 13513–13518. https://doi.org/10.1021/jacs.1c07240
24. Shchepinov, M. S., Udalova, I. A., Bridgman, A. J., & Southern, E. M. (1997). Oligonucleotide dendrimers: Synthesis and use as polylabelled DNA probes. *Nucleic Acids Research, 25*(22), 4447–4454. https://doi.org/10.1093/nar/25.22.4447
25. Ngo, K. H., Distler, M. E., Evangelopoulos, M., Ocampo, T. A., Ma, Y., Minorik, A. J., & Mirkin, C. A. (2025). DNA dendron tagging as a universal way to deliver proteins to cells. *Journal Of The American Chemical Society, 147*(2), 2129–2136. https://doi.org/10.1021/jacs.4c16205
26. Patel, P. C., Giljohann, D. A., Daniel, W. L., Zheng, D., Prigodich, A. E., & Mirkin, C. A. (2010). Scavenger receptors mediate cellular uptake of polyvalent oligonucleotide-functionalized gold nanoparticles. *Bioconjugate Chemistry*, *21*(12), 2250–2256. https://doi.org/10.1021/bc1002423
27. Choi, C. H. J., Hao, L., Narayan, S. P., Auyeung, E., & Mirkin, C. A. (2013). Mechanism for the endocytosis of spherical nucleic acid nanoparticle conjugates. *Proceedings of the National Academy of Sciences of the United States of America, 110*(19), 7625–7630. https://doi.org/10.1073/pnas.1305804110
28. Callmann, C. E., Vasher, M. K., Das, A., Kusmierz, C. D., & Mirkin, C. A. (2023). In vivo behavior of ultrasmall spherical nucleic acids. *Small, 19*(24), Article 2300097. https://doi.org/10.1002/smll.202300097
29. Seferos, D. S., Prigodich, A. E., Giljohann, D. A., Patel, P. C., & Mirkin, C. A. (2009). Polyvalent DNA nanoparticle conjugates stabilize nucleic acids. *Nano Letters*, *9*(1), 308–311. https://doi.org/10.1021/nl802958f
30. Barnaby, S. N., Perelman, G. A., Kohlstedt, K. L., Chinen, A. B., Schatz, G. C., & Mirkin, C. A. (2016). Design considerations for RNA spherical nucleic acids (SNAs). *Bioconjugate Chemistry, 27*(9), 2124–2131. https://doi.org/10.1021/acs.bioconjchem.6b00350
31. Giljohann, D. A., Seferos, D. S., Patel, P. C., Millstone, J. E., Rosi, N. L., & Mirkin, C. A. (2007). Oligonucleotide loading determines cellular uptake of DNA-modified gold nanoparticles. *Nano Letters*, *7*(12), 3818–3821. https://doi.org/10.1021/nl072471q
32. Massich, M. D., Giljohann, D. A., Seferos, D. S., Ludlow, L. E., Horvath, C. M., & Mirkin, C. A. (2009). Regulating immune response using polyvalent nucleic acid-gold nanoparticle conjugates. *Molecular Pharmaceutics*, *6*(6), 1934–1940. https://doi.org/10.1021/mp900172m
33. Bousmail, D., Amrein, L., Fakhoury, J. J., Fakih, H. H., Hsu, J. C. C., Panasci, L., & Sleiman, H. F. (2017). Precision spherical nucleic acids for delivery of anticancer drugs. *Chemical Science*, *8*(9), 6218–6229. https://doi.org/10.1039/C7SC01619K
34. Chinen, A. B., Guan, C. M., Ko, C. H., & Mirkin, C. A. (2017). The impact of protein corona formation on the macrophage cellular uptake and biodistribution of spherical nucleic acids. *Small (Weinheim an der Bergstrasse, Germany), 13*(16), Article 1603847. https://doi.org/10.1002/smll.201603847

35. Zhang, W., Meckes, B., & Mirkin, C. A. (2019). Spherical nucleic acids with tailored and active protein coronae. *ACS Central Science, 5*(12), 1983–1990. https://doi.org/10.1021/acscentsci.9b01105
36. Luczkowiak, J., Muñoz, A., Sánchez-Navarro, M., Ribeiro-Viana, R., Ginieis, A., Illescas, B. M., Martín, N., Delgado, R., & Rojo, J. (2013). Glycofullerenes inhibit viral infection. *Biomacromolecules, 14*(2), 431–437. https://doi.org/10.1021/bm3016658
37. Muñoz, A., Sigwalt, D., Illescas, B. M., Luczkowiak, J., Rodríguez-Pérez, L., Nierengarten, I., Holler, M., Remy, J. S., Buffet, K., Vincent, S. P., Rojo, J., Delgado, R., Nierengarten, J. F., & Martín, N. (2016). Synthesis of giant globular multivalent glycofullerenes as potent inhibitors in a model of Ebola virus infection. *Nature Chemistry, 8*(1), 50–57. https://doi.org/10.1038/nchem.2387
38. Abellán Flos, M., García Moreno, M. I., Ortiz Mellet, C., García Fernández, J. M., Nierengarten, J. F., & Vincent, S. P. (2016). Potent glycosidase inhibition with heterovalent fullerenes: Unveiling the binding modes triggering multivalent inhibition. *Chemistry – A European Journal, 22*(32), 11450–11460. https://doi.org/10.1002/chem.201601673
39. Trinh, T. M. N., Holler, M., Schneider, J. P., García-Moreno, M. I., García Fernández, J. M., Bodlenner, A., Compain, P., Ortiz Mellet, C., & Nierengarten, J. F. (2017). Construction of giant glycosidase inhibitors from iminosugar-substituted fullerene macromonomers. *Journal of Materials Chemistry B, 5*(32), 6546–6556. https://doi.org/10.1039/C7TB01052D
40. Zhang, K., Hao, L., Hurst, S. J., & Mirkin, C. A. (2012). Antibody-linked spherical nucleic acids for cellular targeting. *Journal of the American Chemical Society, 134*(40), 16488–16491. https://doi.org/10.1021/ja306854d
41. Liu, N., Tang, M., & Ding, J. (2020). The interaction between nanoparticles-protein corona complex and cells and its toxic effect on cells. *Chemosphere,* Article 245125624. https://doi.org/10.1016/j.chemosphere.2019.125624
42. Barbalinardo, M., Bertacchini, J., Bergamini, L., Magarò, M. S., Ortolani, L., Sanson, A., Palumbo, C., Cavallini, M., & Gentili, D. (2021). Surface properties modulate protein corona formation and determine cellular uptake and cytotoxicity of silver nanoparticles. *Nanoscale*, *13*(33), 14119–14129. https://doi.org/10.1039/D0NR08259G
43. Schindelin, J., Arganda-Carreras, I., Frise, E., Kaynig, V., Longair, M., Pietzsch, T., Preibisch, S., Rueden, C., Saalfeld, S., Schmid, B., Tinevez, J. Y., White, D. J., Hartenstein, V., Eliceiri, K., Tomancak, P., & Cardona, A. (2012). Fiji: An open-source platform for biological-image analysis. *Nature Methods, 9*(7), 676–682. https://doi.org/10.1038/nmeth.2019
44. Ning, X., Temming, R. P., Dommerholt, J., Guo, J., Ania, D. B., Debets, M. F., Wolfert, M. A., Boons, G. J., & Van Delft, F. L. (2010). Protein modification by Strain-Promoted Alkyne–Nitrone Cycloaddition. *Angewandte Chemie International Edition, 49*(17), 3065–3068. https://doi.org/10.1002/anie.201000408
45. Connors, K. A. (1987). *Binding Constants: The Measurement of Molecular Complex Stability*. John Wiley & Sons.
46. Michel, D. (2007). Cooperative equilibrium curves generated by ordered ligand binding to multi-site molecules. *Biophysical Chemistry, 129*(2–3), 284–288. https://doi.org/10.1016/j.bpc.2007.06.010
47. Gelamo, E. L., & Tabak, M. (2000). Spectroscopic studies on the interaction of bovine (BSA) and human (HSA) serum albumins with ionic surfactants. *Spectrochimica Acta Part A, Molecular and Biomolecular Spectroscopy, 56*(11), 2255–2271. https://doi.org/10.1016/S1386-1425(00)00313-9
48. Nanduri, V., Sorokulova, I. B., Samoylov, A. M., Simonian, A. L., Petrenko, V. A., & Vodyanoy, V. (2007). Phage as a molecular recognition element in biosensors immobilized by physical adsorption. *Biosensors & Bioelectronics*, *22*(6), 986–992. https://doi.org/10.1016/j.bios.2006.03.025
49. Gelamo, E. L., Silva, C. H. T. P., Imasato, H., & Tabak, M. (2002). Interaction of bovine (BSA) and human (HSA) serum albumins with ionic surfactants: Spectroscopy and modelling. *Biochimica et Biophysica Acta (BBA) - Protein Structure and Molecular Enzymology, 1594*(1), 84–99. https://doi.org/10.1016/S0167-4838(01)00287-4
50. López-Hernández, T., Haucke, V., & Maritzen, T. (2020). Endocytosis in the adaptation to cellular stress. *Cell Stress*, *4*(10), 230. https://doi.org/10.15698/cst2020.10.232